Computations of CO_2 Laser Radiation Absorption in SF_6-Air Boundary Layers

JOHN D. ANDERSON JR.*
University of Maryland, College Park, Md.

Numerical results are presented for the absorption of CO_2 laser radiation in SF_6-air laminar compressible boundary layers. The sonic flow over a flat plate at sea level is considered, wherein SF_6 is injected into the boundary layer through the surface, and CO_2 laser radiation at 10.6μ is incident on the plate downstream of the injection. Detailed boundary-layer profiles, the variation of radiative intensity within the boundary layer, and the amount of laser radiation penetrating to the surface is studied using a difference-differential solution of the nonsimilar boundary-layer equations. In the results, strong coupling between the boundary-layer flow and the laser radiation is observed. Because of laser heating of the gas, the attenuation of the radiative intensity within the boundary layer is reduced. As a result, the laser intensity reaching the surface increases nonlinearly with the downstream distance. A limited comparison of the present results with existing experimental data yields good agreement. These results bear on the protection of surfaces from laser beams, such as in new welding techniques, and in laser-gasdynamic energy conversion schemes.

Introduction

SINCE the advent of CO_2-N_2 gasdynamic lasers in 1966,[1] high-energy continuous wave lasers have become a modern reality. In turn, these lasers show great potential for future use in energy transfer and energy conversion schemes. The photon engine discussed by Hertzberg et al.[2] is one such example. The tailoring of aerodynamic flowfields by laser energy addition discussed by Anderson et al.[3] is another. The present investigation is in the latter vein; its purpose is to compute and study the radiative-gasdynamic interaction associated with the absorption of laser radiation in an aerodynamic boundary layer. Specifically, a study is made of SF_6 mass injection into a compressible laminar air boundary layer on a flat plate, with CO_2 laser radiation incident on the boundary layer downstream of the injection. The amount of laser energy absorbed within the SF_6-air boundary layer is calculated, the effects of this radiation on the gasdynamic properties of the flow are studied, and the amount of laser radiation penetrating to the surface is obtained. These results have applications to the protection of surfaces from laser beams, such as in new welding techniques, and in laser-gasdynamic energy conversion schemes.

It is important to note that initial *experimental* results for CO_2 laser radiation absorption in SF_6-air binary boundary layers[3] and in SF_6-air mixtures in absorption cells[4] have already been obtained. These data show that such mixtures and boundary layers can be strong absorbers of CO_2 laser radiation. The present numerical study is carried out in order to complement these experiments.

Analysis

Physical Problem

Referring to the sketch in Fig. 1, consider the flow of air over a flat plate wherein SF_6 is injected into the boundary layer through the surface. Also consider a CO_2 laser beam incident on the outer edge of the boundary layer downstream of the injection. Due to the large absorption coefficient of SF_6 at 10.6μ,[3,4] the laser beam will be attenuated within the boundary layer. In turn, the gasdynamic properties of the boundary layer will be affected. Of particular importance is the temperature increase within the boundary layer. Because the absorption coefficient varies with temperature, and the temperature depends on the amount of radiation absorbed, the flowfield and the radiative intensity distribution are fully coupled. Therefore, the objective is to obtain a numerical solution of the boundary-layer equations for the problem shown in Fig. 1, yielding results for the variation of laser intensity through the boundary layer, as well as detailed profiles of velocity, temperature, and SF_6 mass fraction. All physical properties such as Prandtl number Pr, Lewis number Le, specific heat C_p (including vibrational excitation), and the $\rho\mu$ product are calculated at each local point, and hence, vary through the boundary layer.

The laser radiation is absorbed by several vibrational transitions within the SF_6 molecule,[3,4] thus increasing the vibrational energy of the gas mixture. Some of this energy is transferred to the translational and rotational energies of the gas by way of molecular collisions. In the present analysis, these collisions will be assumed rapid enough that local thermodynamic equilibrium prevails, i.e., the translational, rotational, and vibrational energies of the gas mixture are in equilibrium. This will not be the case if the incident laser intensity is high enough and/or the gas density is low enough that saturation

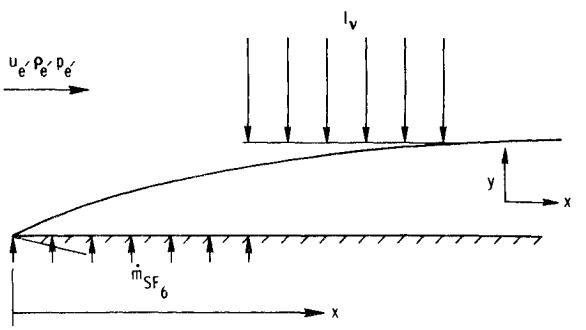

Fig. 1 Physical problem.

Received February 1, 1974; revision received May 17, 1974. Part of this work was performed during the author's employment at the Naval Ordnance Lab., White Oak, Md., and was supported by the NOL Independent Research Program, Problem IR-188. Part was also supported by the Department of Aerospace Engineering, University of Maryland.

Index categories: Lasers; Radiatively Coupled Flows and Heat Transfer.

* Professor and Chairman, Department of Aerospace Engineering. Associate Fellow AIAA.

effects become noticeable; for this situation, the laser radiation absorption will induce vibrational nonequilibrium effects in the gase. Estimates of the intensity required for the onset of saturation are made in Refs. 3 and 4. Based on these estimates, saturation effects were judged not a factor in the experimental data of Refs. 3 and 4. Since the present analysis is a complementary study, the assumption of local thermodynamic equilibrium is particularly appropriate.

Boundary-Layer Equations

For the two-dimensional flow of a compressible, laminar, multicomponent boundary layer with radiative absorption, the governing equations are[5]

Continuity:

$$\frac{\partial(\rho u)}{\partial x}+\frac{\partial(\rho v)}{\partial y}=0 \tag{1}$$

Species Continuity:

$$\rho u\frac{\partial C_i}{\partial x}+\rho v\frac{\partial C_i}{\partial y}+\frac{\partial}{\partial y}(\rho_i V_i)=0 \tag{2}$$

Momentum:

$$\rho u\frac{\partial u}{\partial x}+\rho v\frac{\partial u}{\partial y}=-\frac{\partial p}{\partial x}+\frac{\partial}{\partial y}\left(\mu\frac{\partial u}{\partial y}\right) \tag{3}$$

Energy:

$$\rho u\frac{\partial h}{\partial x}+\rho v\frac{\partial h}{\partial y}=\frac{\partial}{\partial y}\left(k\frac{\partial T}{\partial y}\right)-\frac{\partial}{\partial y}\left(\sum_i \rho_i V_i h_i\right)-\frac{\partial q_R}{\partial y}+\mu\left(\frac{\partial u}{\partial y}\right)^2+u\frac{\partial p}{\partial x} \tag{4}$$

where $\rho_i V_i$ is the diffusion mass flux of species i in the y-direction, x and y are the boundary-layer coordinates shown in Fig. 1, and the remaining notation is standard boundary-layer nomenclature. For a binary mixture of SF_6 and air, Fick's law holds, i.e., $\rho_i V_i=-\rho D_{12}\,\partial C_i/\partial y$. Hence, Eq. (2) becomes

$$\rho u\frac{\partial C_a}{\partial x}+\rho v\frac{\partial C_a}{\partial y}=\frac{\partial}{\partial y}\left(\rho D_{12}\frac{\partial C_a}{\partial y}\right) \tag{5}$$

with

$$C_a+C_{SF_6}=1 \tag{6}$$

where C_a and C_{SF_6} are the mass fractions of air and SF_6, respectively.

With the additional assumption of local thermodynamic equilibrium, and changing to temperature rather than enthalpy as the dependent variable, Eq. (4) becomes[6]

$$\rho u C_p\frac{\partial T}{\partial x}+\rho v C_p\frac{\partial T}{\partial y}=\frac{\partial}{\partial y}\left(k\frac{\partial T}{\partial y}\right)+\rho D_{12}\frac{\partial C_a}{\partial y}\left(\tfrac{7}{2}R_a-4R_{SF_6}-\frac{\partial evib_{SF_6}}{\partial T}\right)\frac{\partial T}{\partial y}-\frac{\partial q_R}{\partial y}+\mu\left(\frac{\partial u}{\partial y}\right)^2+u\frac{\partial p}{\partial x} \tag{7}$$

where R_a and R_{SF_6} are the specific gas constants for air and SF_6, respectively. In Eq. (7), the radiative absorption term, $-\partial q_R/\partial y$, is obtained from the radiative transfer equation [see, e.g., Appendix A of Ref. 7]. If absorption is the only radiative process occurring within the gas, the transfer equation is

$$dI_\nu/dy=-\alpha_\nu I_\nu \tag{8}$$

where α_ν is the linear absorption coefficient of the gas mixture, and I_ν is the local radiative intensity. The term $\alpha_\nu I_\nu$ physically represents the energy absorbed at a local point in the gas/sec/unit volume, hence

$$-\partial q_R/\partial y=-dI_\nu/dy=\alpha_\nu I_\nu \tag{9}$$

Thus, the equations to be solved are Eqs. (1, 3, and 5–7). These are nonlinear, coupled partial differential equations, and must be solved numerically. In establishing a grid network for the numerical solution, accuracy demands that a number of unevenly spaced grid points be concentrated in the regions of high flowfield gradients near the wall, whereas convenience in carrying out the solution suggests an evenly spaced grid. Thus, the independent variables x and y are transformed to ξ and η such that an even grid spacing in the transformed space yields the proper uneven spacing in physical space, as follows:

$$\xi=\int_0^x \rho_e u_e \mu_e\,dx \tag{10}$$

$$\eta=\frac{u_e}{(2\xi)^{1/2}}\int_0^y \rho\,dy \tag{11}$$

This is the standard Lees-Dorodnitzn transformation employed in high-speed boundary-layer theory.[5] For added convenience, the dependent variables are transformed as follows:

$$f'=u/u_e \qquad z=C_a/C_{a_e}$$
$$\theta=T/T_e \qquad \phi=\rho\mu/\rho_e\mu_e$$

After a detailed transformation[6] the resulting equations are

Momentum:

$$(\phi f'')'+ff''+\frac{2\xi}{u_e}\frac{\partial u_e}{\partial\xi}\left[\frac{\rho_e}{\rho}-(f')^2\right]=2\xi\left(f'\frac{\partial f'}{\partial\xi}-f''\frac{\partial f}{\partial\xi}\right) \tag{12}$$

Species Continuity:

$$\left[\frac{Le}{Pr}\phi z'\right]'+fz'-\left(\frac{2\xi}{C_{a_e}}\frac{\partial C_{a_e}}{\partial\xi}\right)f'z=2\xi\left(f'\frac{\partial z}{\partial\xi}-z'\frac{\partial f}{\partial\xi}\right) \tag{13}$$

Energy:

$$\left(\frac{\phi}{Pr}C_p\theta'\right)'+\frac{Le}{Pr}\phi C_{a_e}\left(\frac{7}{2}R_a-4R_{SF_6}-\frac{\partial e_{vibSF_6}}{\partial T}\right)\theta' z'+C_p f\theta'+\phi\frac{u_e^2}{T_e}(f'')^2=2\xi\left[C_p f'\frac{\partial\theta}{\partial\xi}-\frac{\partial f}{\partial\xi}C_p\theta'-\frac{\alpha_\nu I_\nu}{\rho_e u_e^2\mu_e\rho T_e}\right] \tag{14}$$

where the prime denotes partial differentiation with respect to η; i.e., $f'=\partial f/\partial\eta$, and where $L_e=\rho D_{12}C_p/k$, $Pr=\mu C_p/k$ and $\phi=\rho\mu/\rho_e\mu_e$.

Equations (12–14) are still nonlinear partial differential equations. Moreover, referring to Fig. 1, a constant mass injection rate of SF_6 and the incident radiation both preclude a self-similar solution of the equations, i.e., the present problem deals with a *nonsimilar* boundary layer.

Boundary Conditions

At the wall, where $y=0$, $u=u_w=0$, $C_a=C_{a_w}$, and $T=T_w$. The wall temperature, T_w, is assumed constant for the present solutions. The air mass fraction at the wall, C_{a_w}, is unknown and must be solved as part of the solution. In addition, the physical assumption that the wall is impermeable to air yields a boundary condition on the gradient of mass fraction as follows. The mass motion of the air, v_a, is the sum of the mass average velocity for the mixture, v, and the diffusion velocity, V_a, i.e., $v_a=v+V_a$. At the wall, $v_a=0$ due to the impermeable (to air) surface. Hence, at the wall,

$$v=v_w=-V_a=(D_{12}/C_a)(\partial C_a/\partial y) \tag{15}$$

Finally, the mass motion of the mixture at the wall, v_w, can be found from the definition of mass averaged velocity

$$v_w=\sum_i\frac{\rho_i}{\rho}v_i=\left(\frac{\rho_a}{\rho}v_a\right)_w+\left(\frac{\rho_{SF_6}}{\rho}v_{SF_6}\right)_w \tag{16}$$

Since $(v_a)_w=0$, then Eq. (16) yields

$$(\rho v)_w=(\rho_{SF_6}v_{SF_6})_w=\dot m_{SF_6} \tag{17}$$

where $\dot m_{SF_6}$ is the mass injection rate of SF_6 through the surface. Equation (17) is also obvious from a simple mass balance at the surface. Combining Eqs. (15) and (17),

$$\left(\frac{\partial C_a}{\partial y}\right)_w=\left(\frac{C_a}{\rho D_{12}}\right)_w\dot m_{SF_6} \tag{18}$$

For a known $\dot{m}_{SF_6}$, Eq. (18) imposes a boundary condition on the gradient of mass fraction at the wall in terms of the unknown C_{a_w}.

The boundary conditions at the edge of the boundary layer, where $y \to \infty$, are

$$u \to u_e$$
$$C_a \to C_{a_e}$$
$$T \to T_e$$

In terms of the transformed variables, the above boundary conditions are as follows. At the surface, where $\eta = 0$,

$$f' = 0 \tag{19}$$

$$f = -\frac{1}{(2\xi)^{1/2}} \int_0^x \dot{m}_{SF_6}\, dx \text{ in the injection region}$$
$$= 0 \text{ with no injection} \tag{20}$$

$$z_w' = (2\xi)^{1/2} \frac{v_w}{\rho_w u_e D_{12}} z_w \tag{21}$$

$$\theta_w = T_w/T_e \tag{22}$$

At the boundary-layer edge, where $\eta \to \infty$

$$f' \to 1$$
$$z \to 1$$
$$\theta \to 1$$

Transport Properties

The viscosity coefficient for air is taken from Sutherland's Law

$$\mu_a = 1.452 \times 10^{-6}[T^{3/2}/(T+110)] \tag{23}$$

and for SF_6, from Ref. (8),

$$\mu_{SF_6} = 0.0142 \times 10^{-3} + 5.49 \times 10^{-18}(T-273) \tag{24}$$

where μ_a and μ_{SF_6} are in kg/[(m)(sec)] and T is in K. The viscosity coefficient for the mixture, μ, is obtained from Wilke's mixture rule[9] yielding

$$\mu = \mu_a/\{1+0.323(X_{SF_6}/X_a)[1+1.498(\mu_a/\mu_{SF_6})^{1/2}]^2\} + \mu_{SF_6}/\{1+0.144(X_a/X_{SF_6})[1+0.668(\mu_{SF_6}/\mu_a)^{1/2}]^2\} \tag{25}$$

where X_a and X_{SF_6} are the mole fractions for air and SF_6, respectively.

The thermal conductivity for air, k_a, is obtained by assuming that $Pr_a = \mu_a Cp_a/k_a = 0.69$, which is an average value over a temperature range from 0 to 1100 K.[10] The present investigation is limited to this temperature range because, above 1100 K, SF_6 begins to decompose; the effect of such chemical reactions are not treated here. With the additional fact that $Cp_a = 1000$ joules/(kgm)(K) the thermal conductivity for air is

$$k_a = 1450\,\mu_a \text{ joules/(m)(sec)(K)} \tag{26}$$

From Ref. 8, the thermal conductivity for SF_6 is

$$k_{SF_6} = 6.44 \times 10^{-5} T^{0.942} \text{ joules/(m)(sec)(K)} \tag{27}$$

From Mason and Saxena,[11] the thermal conductivity for the mixture, k, is

$$k = k_a/\{1+0.343(X_{SF_6}/X_a)[1+1.5(\mu_a/\mu_{SF_6})^{1/2}]^2\} + k_{SF_6}/\{1+0.153(X_a/X_{SF_6})[1+0.666(\mu_{SF_6}/\mu_a)^{1/2}]^2\} \tag{28}$$

The binary diffusion coefficient is obtained from Reid and Sherwood[12] as follows. From kinetic theory

$$D_{12} = 0.001858 T^{3/2} \left(\frac{m_1+m_2}{m_1 m_2}\right)^{1/2} \Big/ p\sigma_{12}^2 \Omega_D \text{ (cm}^2\text{/sec)} \tag{29}$$

where T is in K, p is in atm, σ_{12} is the collision diameter between two different particles 1 and 2 in Å, Ω_D is the collision integral, and m_1 and m_2 are the molecular weights of the two different species. For SF_6-air mixtures, $[(m_1+m_2)]^{1/2} = 0.205$. Moreover, since SF_6 and air are nonpolar gases with individual collision diameters of 5.128 Å and 3.711 Å, respectively,[12] the combination rule gives $\sigma_{12} = \frac{1}{2}(\sigma_1+\sigma_2) = 4.42$ Å. Also from Ref. (12), $\Omega_D = 1.04$. Thus, the binary diffusion coefficient for SF_6-air mixtures is obtained from Eq. (29) as

$$D_{12} = 1.875 \times 10^{-9}(T^{3/2}/p) \text{ (m}^2\text{/sec)} \tag{30}$$

where D_{12} is in m^2/sec, T is in K and p is in atm.

Absorption Coefficient

Air is essentially transparent at 10.6μ, thus the mixture absorption coefficient is due only to absorption by SF_6. The slight absorption due to CO_2 and H_2O in air is ignored here. However, the SF_6 absorption coefficient is influenced by air through pressure broadening of the individual radiative transitions, or lines; in principle, the line broadening due to SF_6–SF_6 collisions may be different from line broadening due to SF_6-air collisions. To the author's knowledge, Refs. 3 and 4 contain the only data on the absorption coefficient for SF_6-air mixtures; moreover, the data were obtained at near-atmospheric pressures pertinent to the present aerodynamic application. (Measurements of the pure SF_6 absorption coefficient have been obtained previously, but at low pressures, generally less than 1 torr. (See Refs. 3 and 4 for a review of the existing data.) Moreover, the data of Refs. 3 and 4 indicate that CO_2 laser radiation at 10.6μ is absorbed by many overlapping vibrational-rotational lines in SF_6, with the result that α_ν for the mixture is linearly proportional to the number density, hence pressure of SF_6. These data also imply that the pressure broadening cross sections for SF_6-air collisions and for SF_6-SF_6 collisions are essentially the same. In addition, the data of Refs. 3 and 4 contain the only measured temperature variations of α_ν for SF_6, albeit over a moderate range of T. These results show an almost linear decrease in α_ν with increasing T over a range from 300 to 360 K.

In light of the preceding results, the values for α_ν used in the present investigation are obtained from the experimental data of Refs. 3 and 4. Specifically, for SF_6, $\alpha_\nu = 35.4$ m^{-1} torr^{-1} at room temperature. The temperature variation is obtained from the experimental data, with a linear extrapolation to temperatures above 360 K. The equation used for α_ν is

$$\alpha_\nu = p_{SF_6}(5.64 \times 10^4 - 98.5T) \tag{31}$$

where p_{SF_6} is the partial pressure of SF_6 in atm, T is in K, and α_ν is in m^{-1}. This equation is very tenuous because additional hot band transitions may have an effect at higher temperatures, and hence the absorption coefficient may be larger than the present linear extrapolation indicates. In fact according to Eq. (31), α_ν goes to 0 at $T = 573$ K. For $T > 573$ K, $\alpha_\nu = 0$ in the present calculations. The temperature variation of α_ν is the greatest uncertainty in the present analysis.

Radiative Intensity

The distribution of I_ν through the boundary layer is simply obtained from the radiative transfer equation, Eq. (8). This equation is coupled with, and integrated simultaneously with, the boundary-layer equations, as described in the section on the numerical technique. At the boundary-layer outer edge, I_ν is given; at the wall, I_ν is one of the unknowns, and is obtained as part of the solution. The wall is assumed to be nonreflecting.

Thermodynamic Properties

In Eq. (14), $e_{vib_{SF_6}}$ is the vibrational energy of the SF_6.

$$e_{vib_{SF_6}} = \sum_{i=1}^{6} \frac{g_{\nu_i}(h\nu_i/k)R_{SF_6}}{e^{h\nu_i/kT}-1} \tag{32}$$

where the sum is taken over the six vibrational modes of SF_6, and where the statistical weights g_{ν_i} and fundamental frequencies are given in Table 1, obtained from Ref. 3.

The mixture specific heat, C_p, in Eq. (14) is $C_p = C_a C_{p_a} + C_{SF_6} C_{p_{SF_6}}$.

$$\text{Air:} \quad C_{p_a} = 7R_a/2$$
$$SF_6: \quad C_{p_{SF_6}} = 4R_{SF_6} + \partial(e_{vib_{SF_6}})/\partial T$$

Table 1 Fundamental vibrational frequencies and degeneracies for SF_6

Mode	Fundamental frequency (cm^{-1})	Degeneracy
ν_1	770	1
ν_2	640	2
ν_3	948	3
ν_4	614	3
ν_5	522	3
ν_6	350	3

Numerical Technique

The present analysis deals with nonsimilar boundary layers; this nonsimilarity is due to the constant mass injection rate of SF_6 at the surface of the flat plate, and the constant radiative intensity incident at the outer edge. The present numerical approach is patterned after the difference-differential method suggested by Smith, Clutter, and Jaffe.[13–15] Here, the partial derivatives in the flow direction are replaced by finite-differences. Therefore, Eqs. (12–14) become ordinary differential equations in η, and are solved at each streamwise station by the standard Adams-Moulton predictor-corrector method. For the present results, the FNOL2 subroutine[16] was employed.

Specifically, the flow along the flat plate is divided into a number of equally spaced streamwise stations. At each station, the ξ derivatives in Eq. (12–14) are replaced by (see Fig. 2)

$$\frac{\partial F_n}{\partial \xi} = \frac{3F_n - 4F_{n-1} + F_{n-2}}{2\Delta\xi} \tag{33}$$

where F represents any quantity such as f, f', z, etc. This form for the derivative is suggested in Ref. 13. However, referring to Fig. 2, in order to start the solution, the flow at station (1) is assumed to be "locally similar," i.e., $\partial^F n/\partial\xi = 0$. With these results at Station 1, a simple rearward difference

$$\frac{\partial F_n}{\partial \xi} = \frac{F_n - F_{n-1}}{\Delta\xi}$$

is employed at Station 2. For Station 3 and all other downstream stations, Eq. (33) is used. The need to start the nonsimilar boundary-layer solution from some known profiles, such as a "locally similar" solution near the leading edge, is characteristic of the difference-differential numerical method.[13–15] In the present solution, where mass injection is assumed to start at the leading edge, a "locally similar" solution employing the local $\dot{m}_{SF_6}$ at Station 1, is not totally satisfactory. However, no other recourse is evident. Fortunately, such a starting solution should not compromise the dominant and important effects of the radiative gasdynamic coupling downstream which is the main concern of the present analysis.

At a given streamwise location, with finite-differences for the ξ derivatives, Eqs.(12–14) become ordinary differential equations in η. These equations are solved between the previously described split boundary conditions at the wall and at the edge. Note that Eq. (12) is third order, and Eqs. (13) and (14) are each second order. On the other hand, Eqs. (19–22) provide only four

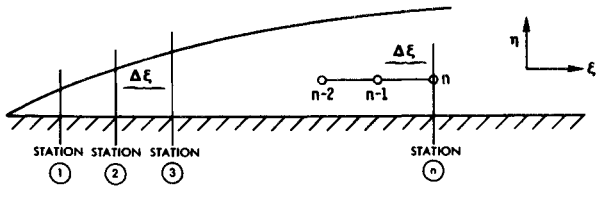

Fig. 2 Numerical grid.

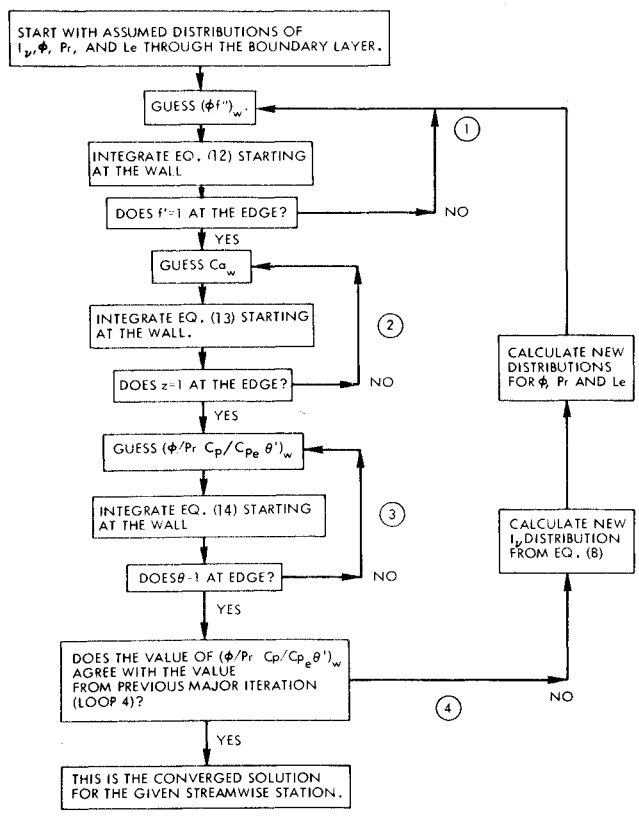

Fig. 3 Numerical iteration scheme.

boundary conditions at the wall. In order to integrate Eqs. (12–14) starting at the wall, three additional wall boundary conditions are assumed, and the results of the integration across the boundary layer are then matched with the boundary conditions at the outer edge. This implies an iterative solution, commonly called the "shooting" technique. A second reason for an iterative solution at each streamwise location is the radiative term in Eq. (14); this term requires a priori knowledge of the local radiative intensity I_ν. After each major iteration which yields a solution of the energy equation, Eq. (14), the radiative transfer equation, Eq. (8), is solved for the distribution of I_ν through the boundary layer, and the results are used in Eq. (14) for each subsequent iteration. For clarity, the over-all iterative scheme is diagramed in Fig. 3; the iterative solution requires several minor iterations nested within a major iteration.

An important comment must be made with regard to the ease of solution. Referring to Fig. 3, the integration of Eqs. (12–14) is extremely sensitive to the guessed boundary conditions on loops 1, 2, and 3. For example, in some cases the guessed value of $(\phi f'')_w$ must be accurate to at least six significant figures; otherwise, the integration of Eq. (12) will result in infinities before the edge of the boundary layer is reached. This behavior is due to the finite ξ derivatives which act as forcing functions in the equations, and which go to zero at the outer edge for only a very precise guessed value of $(\phi f'')_w$. Numerical machinery is inserted in the program to sense when the solution is diverging at some intermediate point within the boundary layer. Then, a new improved guess for $(\phi f'')_w$ is made, and loop 1 is executed even before the edge of the boundary layer is reached. Similar machinery is required for loops 2 and 3 for the same reasons. This machinery has to be adjusted at each streamwise location and for each different set of freestream conditions. It is the author's experience that the "nursing" required to bring about a converged solution is laborious and time consuming; this represents a serious drawback in the practical use of the present analysis if results for a large number of different cases are desired. For the present investigation, this drawback is not

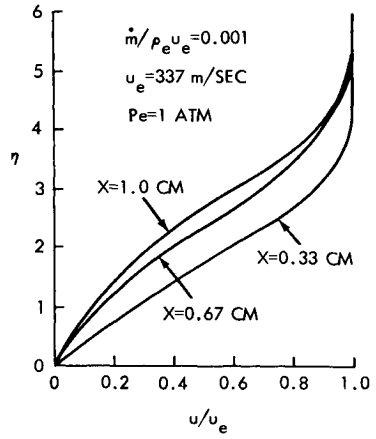

Fig. 4 Velocity profiles in the region of mass injection.

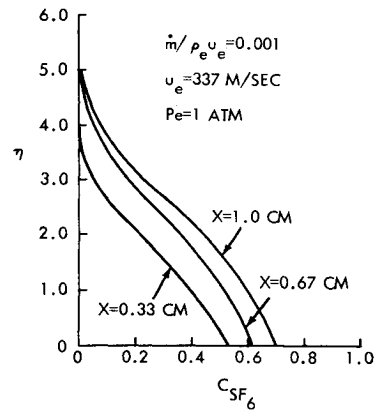

Fig. 6 Mass fraction profiles for SF_6 in the region of mass injection.

serious because the over-all physical phenomena associated with the radiative gasdynamic interaction within the boundary layer are being studied, and therefore results for only a few representative cases are required.

For the present results, a constant value of $\Delta\eta$ is chosen such that 120 points were evenly spaced across the boundary layer. The chosen value of $\Delta\xi$ corresponds to a physical increment of 0.33 cm in the region of mass injection, and 0.2 cm in the region with radiation.

With regard to numerical accuracy, Smith et al.[13-15] have established that the difference-differential technique is accurate for a number of boundary-layer problems over a variety of aerodynamic shapes, with conditions ranging from incompressible flow to the high temperature, nonequilibrium, chemically reacting flow associated with high-speed re-entry. Moreover, as a test case, the present analysis was applied to the known exact solution for the compressible flow of a calorically perfect gas over a flat plate, and the results reproduced very closely those of the exact self-similar solutions of Cohen and Reshotko.[17] Hence, confidence in the numerical accuracy of the present investigation is reasonably high.

Results

In this paper, results are given for a sonic freestream velocity at sea level; i.e., $u_e = 337$ m/sec and $p_e = 1$ atm. Referring again to Fig. 1, a constant SF_6 mass injection rate, $\dot{m}_{SF_6} = 0.001\rho_e u_e$, is assumed from the leading edge to the $x = 1$ cm station. A CO_2 laser beam with a constant intensity of 1000 w/cm^2 is incident normally on the outer edge of the boundary layer, beginning at $x = 1$ cm and extending downstream. Also, $T_w = T_e = 289$ K.

Flowfield Profiles

The velocity profiles through the boundary layer at several stations in the mass injection region are shown in Fig. 4. Note the sharp decrease of the velocity gradient at the wall, $(\partial u/\partial\eta)_w = (f'')_w$, for the downstream stations. Also note the downstream development of a profile that is characteristic of near-separation. This is typical of boundary-layer velocity profiles in regions of mass injection at the wall. The mass injection is terminated at $x = 1$ cm, and in Fig. 5, velocity profiles are shown at two stations downstream of the termination point. Note that these profiles tend to relax to a shape characteristic of a noninjection region. Emphasis is made that the velocity profiles shown in Fig. 5 are fully coupled with the laser radiation, which is incident on the boundary layer beginning at $x = 1$ cm.

The profiles of SF_6 mass fraction, C_{SF_6}, are shown in Fig. 6. For the downstream stations, note the increase of (C_{SF_6}) as well as the developing fullness of the profile due to molecular diffusion. The profiles downstream of the injection termination point are shown in Fig. 7; here, the mechanism of diffusion still maintains a finite $(C_{SF_6})_w$, although the value decreases downstream.

Of particular interest are the temperature profiles in the radiation region; these are shown in Fig. 8, starting at the $x = 1$ cm station. At $x = 1$ cm, the profile of T/T_e is characteristic of a compressible laminar boundary layer, where a local temperature increase within the boundary layer is caused by viscous dissipation. The increase is small, however, because the external velocity (sonic velocity) is moderate. On the other hand, the bulk heating of the gas due to absorption of the laser radiation is strong at $x = 1.2$ and 1.4 cm. Note that large temperature increases and strong temperature gradients are induced within the boundary layer by the radiation. Also, by

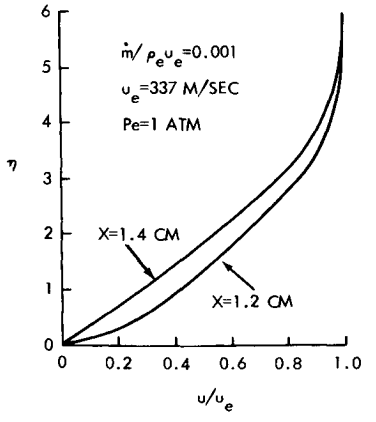

Fig. 5 Velocity profiles in the region of radiation.

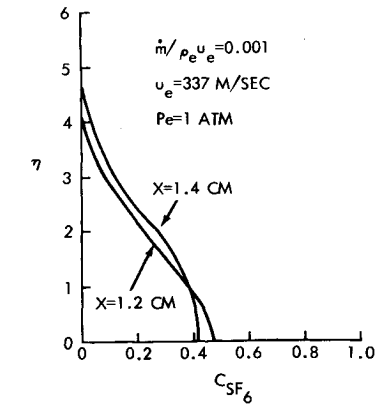

Fig. 7 Mass fraction profiles for SF_6 in the region of radiation.

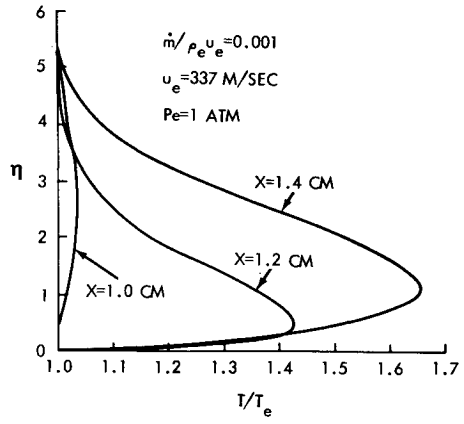

Fig. 8 Temperature profiles in the region of radiation.

comparing the different profiles plotted versus η in Fig. 8, the strong nonsimilarity of the boundary layer is quite evident.

Radiative Intensity

The distribution of radiative intensity through the boundary layer is affected by the temperature increase of the gas. These effects are shown in Fig. 9. Here, the intensity distributions through the boundary layer are given for $x = 1$ cm, which is the leading edge of the laser beam where the gas has not had time to experience any heating, and for $x = 1.4$ cm, which is in the region where strong temperature increases have occurred. Taken as a whole, Figs. 8 and 9 show the essence of the radiative gasdynamic coupling; the radiative absorption affects the gasdynamics, and the gasdynamics affects the radiative absorption. For the case shown, the coupling phenomena are strong, and are clearly a dominant factor for CO_2 laser radiation absorption in SF_6-air boundary layers.

The distribution of surface intensity along the flat plate is shown in Fig. 10. Because of the bulk heating of the gas, α_ν is reduced and the attenuation of the laser beam is weakened with increasing downstream distance. Therefore, the surface intensity increases with distance. In Ref. 3, where data for surface intensity were obtained with a laser beam of fixed diameter, it is stated that a nonlinear scaling effect prevented the data from being applied to larger laser beams. In Fig. 10 the source of this nonlinear scaling effect is quite evident. For a constant incident

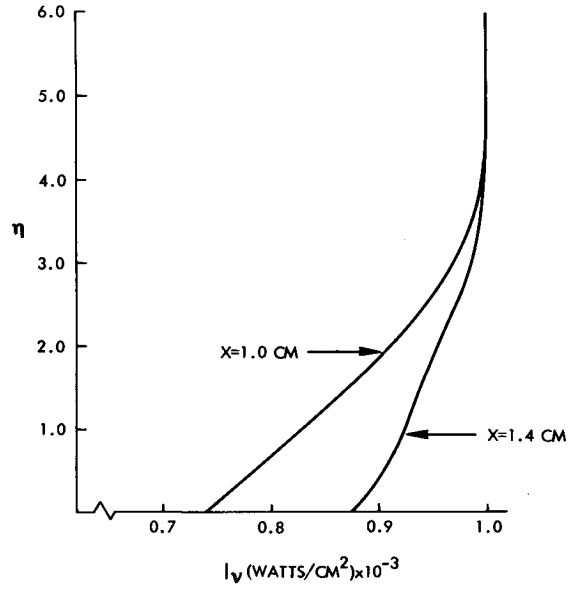

Fig. 9 CO_2 laser radiation intensity profiles through the boundary layer.

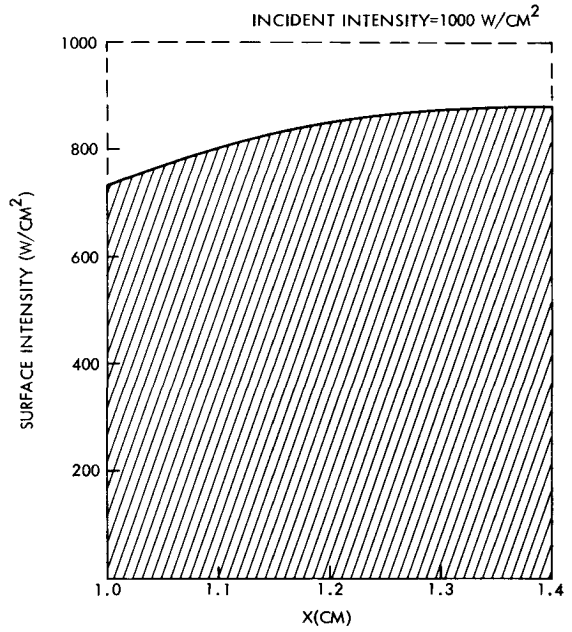

Fig. 10 CO_2 laser radiative intensity distribution along the surface.

intensity, the leading edge of the laser beam will be attenuated the most, and the trailing edge the least. Therefore, the intensity reaching the surface, averaged over the whole laser beam diameter, will depend in a nonlinear fashion on the beam diameter itself.

A comparison between the present analytical results and the experimental data of Ref. 3 for surface intensity cannot be made in a direct and accurate fashion due to the following differences. The experimental data were obtained on the sidewall of a subsonic wind tunnel, where the boundary layer is different from that developed from the leading edge of a flat plate. Moreover, the SF_6 was injected through a circular porous plug of 2.54 cm diam, hence the experimental boundary-layer flow is not truly two-dimensional. In addition, the freestream velocity was 125 m/sec, less than half the sonic velocity employed in the present results. Despite these differences, there are enough similarities that a coarse comparison can be made. In Fig. 10, over a distance of 0.4 cm, the analytical value of the mean surface intensity is about 800w/cm^2. For comparison, the experimental data from Ref. 3 are shown in Fig. 11, along with the above analytical

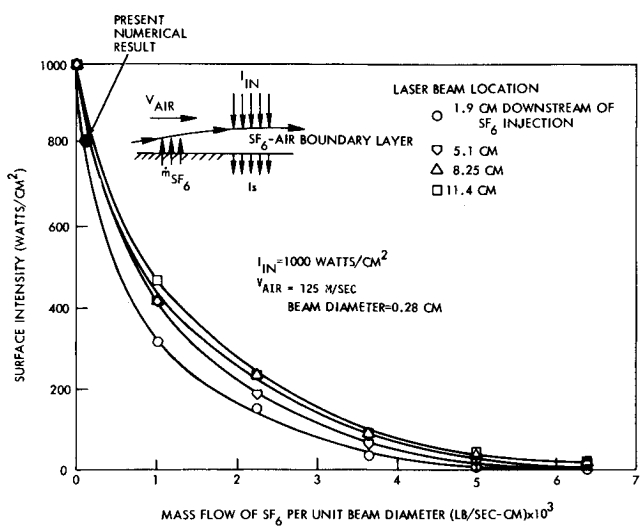

Fig. 11 Experimental variation of surface intensity with mass injection of SF_6[3]; comparison with present theory.

result. For the same SF_6 mass flow through the laser beam per-unit beam diameter, the experimental data also indicate a surface intensity of about 800 w/cm^2. Thus, the present analysis appears to yield reasonable results.

In further regard to the existing experimental data, cases were attempted in the present study for stronger injection rates, i.e., for $\dot{m}_{SF_6}/\rho_e u_e$ larger than 0.001. However, for values of 0.002 and above, the velocity gradient at the wall, $(f'')_w$, went to zero in the iterative process, and the developing velocity profiles indicated boundary-layer separation. The present analysis does not hold for separated flow, and hence no results are presented. However, in light of the present analysis, it now appears likely that a number of the experimental data points shown in Fig. 11 were obtained with the laminar boundary layer blown off the surface.

Convective Heating

Referring again to the temperature profiles shown in Fig. 8, the temperature gradient at the wall, and hence the convective heating (Q_c) to the surface, is markedly increased due to laser radiation absorption in the layers of SF_6 near the cold wall. For example, Q_c in the mass injection region varies from 1.125 w/cm^2 at $x = 0.33$ cm to 0.313 w/cm^2 at $x = 1.0$ cm, whereas Q_c increases markedly to 22.7 w/cm^2 at $x = 1.4$ cm in the region of laser radiative absorption. Unfortunately, results with no laser radiation are not available in the region downstream of the mass injection. Thus, the purely fluid dynamic contributions to Q_c in the relaxation region downstream of the discontinuous termination of injection cannot be separated from the contribution due to laser absorption. Nevertheless, these results indicate that the reduction in laser intensity at the surface due to absorption within the SF_6 may be partly, if not totally, negated by an increase in convective heating. This aspect is important, and is worthy of future study.

Conclusions

The first analytical results are presented for the radiative gasdynamic interaction associated with CO_2 laser radiation absorption in SF_6-air laminar compressible boundary layers. These results clearly show the physical trends and properties associated with the radiatively coupled flow. In particular:

1) Deep within the boundary layer, the temperature is considerably increased due to laser-induced bulk heating of the gas.

2) In turn, this reduces the attenuation of the laser beam within the boundary layer.

3) As a result, the laser intensity at the surface increases nonlinearly with downstream distance.

4) A very limited comparison of the present numerical results for mean surface intensity with existing experimental data yields good agreement.

5) The present analysis deals with a laminar boundary layer; however, results for a turbulent boundary layer should follow the same qualitative trends.

References

[1] Gerry, E. T., "Gasdynamic Lasers," AIAA Paper 71-23, New York, 1971.

[2] Hertzberg, A. et al., "Photon Generators and Engines for Laser Power Transmission," *AIAA Journal*, Vol. 10, No. 4, April 1972, pp. 394–400.

[3] Anderson, J. D. Jr., Wagner, J. L., and Knott, J., "CO_2 Laser Radiation Absorption in SF_6Air Boundary Layers," AIAA Paper No. 73-262, Washington, D.C., 1973; also NOLTR 72-172, Naval Ordnance Laboratory, White Oak, Md., Aug. 1972.

[4] Anderson, J. D. Jr., Wagner, J. L., and Knott, J., "CO_2 Laser Radiation Absorption in SF_6-Air Mixtures," *AIAA Journal*, Vol. 11, No. 10, Oct. 1973, pp. 1424–1426.

[5] Dorrance, W. H., *Viscous Hypersonic Flow*, McGraw-Hill, New York, 1962, pp. 25–26.

[6] Anderson, J. D. Jr., "A Numerical Analysis of CO_2 Laser Radiation Absorption in SF_6-Air Laminar Boundary Layers," NOLTR 73-143, July 1973, Naval Ordnance Lab., White Oak, Md.

[7] Anderson, J. D. Jr., "Nongray Radiative Transfer Effects on the Radiating Stagnation Region Shock Layer and Stagnation Point Heat Transfer," NOLTR 67-104, July 1967, Naval Ordnance Lab., White Oak, Md.

[8] "Sulfur Hexafluoride for Gaseous Insulation," Pamphlet TB-85603, Baker and Adamson Group, General Chemical Division of Allied Chemical N.Y., N.Y.

[9] Wilke, C. R., "A Viscosity Equation for Gas Mixtures," *Journal of Chemical Physics*, Vol. 18, No. 4, April 1950, pp. 517–519.

[10] Eckert, E. R. G. and Drake, R. M. Jr., *Heat and Mass Transfer*, McGraw-Hill, New York, 1959, p. 504.

[11] Mason, E. A. and Saxena, S. C., "Approximate Formula for the Thermal Conductivity of Gas Mixtures," *The Physics of Fluids*, Vol. 1, No. 5, Sept.–Oct. 1958, pp. 361–369.

[12] Reid, R. C. and Sherwood, T. K., *The Properties of Gases and Liquids: Their Estimation and Correlation*, 2nd ed., McGraw-Hill, New York, 1966, pp. 523–529.

[13] Smith, A. M. O. and Clutter, D. W., "Solution of the Incompressible Laminar Boundary Layer Equations," *AIAA Journal*, Vol. 1, No. 9, Sept. 1963, pp. 2062–2071.

[14] Smith, A. M. O. and Clutter, D. W., "Machine Calculation of Compressible Laminar Boundary Layers," *AIAA Journal*, Vol. 3, No. 4, April 1965, pp. 639–647.

[15] Smith, A. M. O. and Jaffe, N. A., "General Method for Solving the Laminar Nonequilibrium Boundary-Layer Equations of a Dissociating Gas," *AIAA Journal*, Vol. 4, No. 4, April 1966, pp. 611–620.

[16] Linnekin, J. S. and Belliveau, L. J., "FNOL2, A Fortran (IBM 7090) Subroutine for the Solution of Ordinary Differential Equations With Automatic Adjustment of the Interval of Integration," NOLTR 63-171, July 1963, Naval Ordnance Lab., White Oak, Md.

[17] Cohen, C. B. and Reshotko, E., "Similar Solutions for the Compressible Laminar Boundary Layer with Heat Transfer and Pressure Gradient," *Recent Advances in Heat and Mass Transfer*, edited by J. P. Hartnett, McGraw-Hill, New York, 1961, pp. 82–114; also Rept. 1293, 1956, NACA.